Pharm Res (2011) 28:2246–2260
DOI 10.1007/s11095-011-0455-0

RESEARCH PAPER

Structure-Skin Permeability Relationship of Dendrimers

Venkata Vamsi Venuganti • Preety Sahdev • Michael Hildreth • Xiangming Guan • Omathanu Perumal

Received: 24 August 2010 / Accepted: 20 April 2011 / Published online: 2 June 2011

ABSTRACT

Purpose To investigate skin penetration of poly (amidoamine) (PAMAM) dendrimers as a function of surface charge and molecular weight in presence and absence of iontophoresis.

Methods Dendrimers were labeled with fluoroisothiocynate (FITC); skin penetration of dendrimers was studied using excised porcine skin *in-vitro*. Skin penetration of FITC-labeled dendrimers was quantified using confocal laser scanning microscope (CLSM). G2-G6 NH_2, G3.5-COOH and G4-OH dendrimers were used.

Results Cationic dendrimers showed higher skin penetration than neutral and anionic dendrimers. Skin penetration of cationic dendrimer increased linearly with increase in treatment time. Iontophoresis enhanced skin penetration of cationic and neutral dendrimers. Increase in current strength and current duration increased skin transport of dendrimers. Passive and iontophoretic skin penetration of cationic dendrimers was inversely related to their molecular weight. Dendrimer penetrated the skin through intercellular lipids and hair follicles. With iontophoresis, dendrimer was also found in localized skin regions.

Conclusions The study demonstrates that the physicochemical properties of dendrimers influence their skin transport. Findings can be used to design dendrimer-based nanocarriers for drug delivery to skin.

KEY WORDS confocal laser scanning microscope · dendrimer charge · dendrimer generation · iontophoresis · nanocarrier

INTRODUCTION

The large surface area (1.8 m^2) and easy accessibility of skin makes it an attractive route for drug delivery. However, the unique bioarchitecture of skin limits the transport of molecules through it (1). Stratum corneum (SC), which is the outer most layer of the skin, is 10–20 μm thick and is made up of stacks of keratin-filled corneocytes interdispersed with tightly arranged lipid bilayers (2). Generally, transdermal delivery is limited to small (<500 Da) lipophilic (Log P 1–3) molecules (3). However, various chemical and physical methods have been used to increase drug penetration and expand the number of drugs delivered through skin (3,4). These include the use of chemical penetration enhancers and physical methods such as use of electric field (iontophoresis, electroporation), ultrasound waves and microneedles (3,4). On the other hand, several micro and nanocarriers are being investigated for transcutaneous delivery of drugs (5,6). These include the use of microemulsions, liposomes, lipid nanoparticles, micelles and polymeric nanoparticles (5,6). As opposed to lipid-based carriers, very little is known about the transport

Electronic Supplementary Material The online version of this article (doi:10.1007/s11095-011-0455-0) contains supplementary material, which is available to authorized users.

P. Sahdev • X. Guan • O. Perumal (✉)
Department of Pharmaceutical Sciences
South Dakota State University
Brookings, South Dakota 57007, USA
e-mail: omathanu.perumal@sdstate.edu

M. Hildreth
Department of Biology and Microbiology
South Dakota State University
Brookings, South Dakota 57007, USA

Present Address:
V. V. Venuganti
Pharmacy Division Birla Institute of Technology and Science
Pilani - Hyderabad Campus Jawahar Nagar
Shameerpet Mandal
Hyderabad, 500078, Andhra Pradesh, India

of polymeric carriers through skin. To this end, the present study focuses on investigating the skin transport of dendritic polymers with the aim of using them as nanocarriers for transcutaneous drug delivery.

Dendrimers are a unique class of branched polymers with well-defined core-shell architecture. They offer distinct advantages as a nanocarrier due to their monodispersity, globular shape, and high density of surface-functional groups (7). Drugs can be encapsulated in the core or complexed or conjugated to the surface-functional groups. Further, the number of surface-functional groups can be easily varied by controlling the number of branching units (i.e. generations). The high density of surface-functional groups in dendrimers results in multivalent interactions with drugs and biological membranes (8,9). Dendrimers have been investigated as drug delivery carriers for various biological membranes (8,10–13). The membrane permeability, biodistribution, and toxicity of dendrimers are dependent on their surface-functional groups, charge, size and generation (10,14,15). Both cationic and anionic dendrimers have been found to cross fully differentiated Caco-2 cells (10,14). On the other hand, neutral hydroxyl-terminated dendrimer showed minimal transport through Caco-2 cells (14). El-Sayed *et al.* (10) reported that dendrimer permeation across fully differentiated Caco-2 cells is dependent on the dendrimer generation, where lower generation dendrimers showed higher permeation than the higher generation dendrimers (10). Further, they also demonstrated that the extravasation time of dendrimer through microvascular endothelium increased with increase in dendrimer generation (16). Cationic dendrimers have been used as efficient transfecting agents for gene delivery (17).

Dendrimers have been reported to increase the skin penetration of lipophilic and hydrophilic drugs (18–20). The skin penetration of 5-fluorouracil was enhanced by cationic dendrimers, which was higher than the penetration enhancement caused by neutral and anionic dendrimers (20). Further, the lower generation cationic dendrimers showed greater penetration enhancement than higher generation dendrimers (20).To design dendrimer-based nanocarriers for transcutaneous drug delivery, it is important to understand *per se* the skin transport of dendrimers. In this work, the skin penetration of dendrimers is studied as a function of their surface charge and generation. Further, the study also demonstrates the feasibility of using dendrimers as charged nanocarriers for transcutaneous iontophoretic drug delivery. Iontophoresis is a physical enhancement technique that uses a small current ($\leq$0.5 mA/cm^2) to transport molecules through skin (21). Excised porcine skin, which is the closest animal model to human skin (22), was used for studying the *in-vitro* skin transport of dendrimers. Dendrimers were labeled with fluouroisothiocyanate (FITC) to characterize the skin transport by confocal laser scanning microscopy (CLSM). The skin penetration of FITC-labeled dendrimer was quantified using the fluorescence intensity in SC and viable epidermis

MATERIALS AND METHODS

Materials

PAMAM dendrimers were purchased from Dendritech Inc., Midland, MI. The properties of dendrimers used in the study are given in Table I. Fluorisothiocyanate (FITC), N-(3-dimethylaminopropyl)-*N*'-ethylcarbodiimide (EDC), ethylene diamine, triethylamine, dimethylformamide (DMF) and all other chemicals were purchased from Sigma-Aldrich chemical company (St. Louis, MO).

FITC Conjugation of Dendrimers

Dendrimer was labeled with FITC, following the method of Kitchens *et al.* (14). FITC was taken in a three-fold molar excess for the conjugation reaction. For amine-terminated dendrimers, FITC (5 mg/mL) was dissolved in acetone and slowly added to the dendrimer in phosphate-buffered saline (PBS; pH 7.4). The reaction mixture was incubated at room temperature for 24 h. For carboxyl-terminated dendrimer, three-fold molar excess of EDC was added to the dendrimer solution and incubated for 30 min. Three times molar excess of ethylene diamine was added to the mixture and incubated for 4 h. FITC (5 mg/mL) was dissolved in acetone and was slowly added to this solution followed by incubation at room temperature for 24 h. For hydroxyl-terminated dendrimer, the conjugation was carried out by dissolving the dendrimer in DMF. Dendrimer, triethylamine, and FITC at a molar ratio of 1:3:3 was incubated in DMF at 80°C for 72 h in a nitrogen atmosphere.

The FITC-dendrimer conjugates were dialyzed against deionized water using nitrocellulose membrane (Mwt cut-off 1–10 kDa; Spectrum laboratories Inc., Rancho Dominguez, CA) to separate the free FITC. The conjugate was further purified by passing through a Sephadex PD10 column (Amersham biosciences, Piscataway, NJ) and stored at 4°C after lyophilization.

Characterization of FITC-Dendrimer Conjugates

The purity of the FITC-dendrimer conjugates was evaluated by thin layer chromatography (TLC) (23). Briefly, 100 μg/ml of FITC-dendrimer conjugate and free FITC were spotted onto a TLC aluminum plate (Silica gel 60F254, Merck kGaA, Darmstadt, Germany). Chloroform: methanol: ammonium hydroxide (5:4:1) was used as the mobile phase to develop the plate in a TLC chamber. After

Table I Physicochemical Properties of PAMAM Dendrimers used in the Study

Surface group	Generation	Size[a] (nm)	Zeta[a] Potential (mv)	Molecular weight (Da)[b]	No. Surface groups[b]	FITC (mM/g dendrimer)	Percent substituted[c]
-NH_2	G_2	10.59 ± 0.7	2.66 ± 1.0	3,256	16	0.0830	1.69%
-NH_2	G_3	13.15 ± 1.0	3.19 ± 0.2	6,909	32	0.0780	1.69%
-NH_2	G_4	14.45 ± 0.8	13.94 ± 1.5	14,215	64	0.3000	6.69%
-NH_2	G_5	16.0 ± 0.9	24.33 ± 1.1	28,826	128	0.0730	1.65%
-NH_2	G_6	18.29 ± 0.9	26.01 ± 1.3	58,048	256	0.1300	2.95%
-COOH	$G_{3.5}$	15.20 ± 0.6	−13.0 ± 1.1	12,931	64	0.0710	1.44%
-OH	G_4	14.74 ± 0.5	−3.4 ± 1.2	14,279	64	0.0091	0.2%

[a] Measured using particle size analyzer. Mean of three measurements ± SD

[b] From www.dendritech.com

[c] Percent of corresponding number of FITC molecules in the dendrimer surface groups

drying the plate, the yellow spots for FITC in the conjugate was visualized by comparing it against free FITC. Infrared spectroscopy and proton NMR were used to confirm FITC conjugation to dendrimers. The IR spectrum was recorded on ZnSe crystal at 2 cm^{-1} resolution in Nicolet 380 ATR-FTIR spectrophotometer (Thermo electron Corporation, Madison, WI). Each spectrum was an average of 100 scans. The peak position was analyzed using OMNIC software. Nuclear magnetic resonance (NMR) spectroscopy was also used to characterize the dendrimer-FITC conjugates. A 5 mg/mL sample was subjected to 500 scans using 400 Hz Bruker NMR (Bruker Daltonics Inc., Fremont, CA). The extent of FITC conjugation was measured in a UV-visible spectrophotometer (Spectra Max, Molecular devices, Sunnyvale, CA) at 495 nm. Number of moles of FITC conjugated per dendrimer was calculated using FITC calibration curve in phosphate-buffered saline (PBS, pH 7.4). The particle size and zeta potential of FITC-labeled dendrimers were measured by dynamic light scattering using Nicomp ZLS 380 particle size analyzer (Nicomp, Santa Barbara, CA).

Preparation of Skin Samples

Porcine ears were obtained from the slaughter house in the Department of Animal and Range Sciences at South Dakota State University. The ears were collected immediately after slaughtering and washed under tap water. Hair on the dorsal side was removed with a hair clipper (Golden A5, Oster, Niles, IL). The skin was excised from the underlying cartilage using scalpel and forceps. Fat adhering to the dermis side was carefully removed using a blunt scalpel, and the skin was observed for any visible damage. Skin was dermatomed to a thickness of 300 μm using a model B electric dermatome (Padgett Instruments, St. Louis, MO). The skin was stored at −20°C and was used within three months.

Measurement of SC Thickness

To determine the thickness of porcine SC, the skin was tape stripped using Scotch book tape (845, 3M, St. Paul, MN) to remove the SC. A skin area of 0.7 cm^2 was used for tape stripping. After each tape strip, the transepidermal water loss (TEWL) was measured. Tape stripping was performed until a significant change in TEWL was observed. Weight of the tape strip was recorded before and after stripping using a microbalance (Sartorius CPA 2P, Bohemia, NY) to estimate the weight of SC removed. The thickness of the SC removed was calculated using the following equation (24):

$$h = \frac{m}{da}$$

where h is the thickness of SC, m is the mass of SC removed, d is the density of skin, and a is the area of the skin used for tape stripping. The density of the skin was assumed to be 1 g/cm^3 (24).

Skin Penetration Studies

Skin was thawed to room temperature and sandwiched between the donor and receptor chambers in a Franz diffusion cell (PermeGear, Hellertown, PA). The receptor chamber was filled with 6 mL of phosphate buffer (PB, pH 7.4) and was stirred using a magnetic stirbar. The receptor medium was maintained at 37°C. Only those skin pieces with a TEWL <10 $g/m^2/h$ and electrical resistance >20 k Ω/cm^2 were used in the study. Donor chamber was loaded with 0.2 mL of 70 μM of FITC-labeled dendrimers. Influence of dendrimer surface charge on skin penetration was studied using G_4-NH_2, $G_{3.5}$-COOH and G_4-OH dendrimers. The dendrimers have positive, negative, and neutral charge, respectively, at pH 7.4 (25). The influence of treatment time on skin penetration of G_4-NH_2 dendrimer was studied by treating the skin for 2, 12 and 24 h.

For studying the effect of dendrimer generation on skin penetration, G_2 to G_6-NH_2 dendrimers were used. At the end of the treatment, the skin samples were washed three times with PBS and mounted on a glass slide for analysis by CLSM. To compare the skin penetration of free FITC and FITC-dendrimer conjugates, the skin was treated with 15 μg/ml of FITC in PBS (this is equivalent to average FITC concentration in FITC-dendrimer conjugates) and then analyzed by CLSM. Since there was a strong FITC fluorescence in the SC, it was difficult to differentiate the fluorescence between free and dendrimer-conjugated FITC. Therefore, in a separate experiment after treatment with FITC and G_4-NH_2-FITC conjugate (15 μg/ml equivalent of FITC), the skin was tape stripped to remove SC. Then the tape-stripped skin was observed under fluorescence microscope.

Measurement of TEWL and Skin Resistance

The TEWL (gm/m^2/h) was measured by placing the vapometer (Delfin Technologies, Kuopio, Finland) on the donor chamber. For measuring the skin resistance, a direct current of 0.3 mA/cm^2(I) was applied using a constant power supply unit (Phoresor II, Iomed, Inc, UT) and Ag/AgCl electrodes (*In-vivo* metric, Healdsburg, CA). The potential difference (V) across the skin was measured using a multimeter (Fluke 189, FlukeEverett, WA). The skin resistance (R) was calculated from Ohm's law ($V = IR$) (26).

Iontophoresis Application

For iontophoretic studies, a current density of 0.31 mA/cm^2 was applied for 2 h using a constant power supply unit (Phoresor II, Iomed Inc., Salt Lake City, UT) with Ag/AgCl electrodes (*In-vivo* metric, Healdsburg, CA). For cationic and neutral dendrimers, the anode was placed in the donor chamber and cathode in the receptor chamber. In case of anionic dendrimer, either anode or cathode was placed on the donor chamber. The effect of current density and current duration on skin penetration of dendrimers was studied using G_4-NH_2 dendrimer. Current density was varied from 0.31 to 0.47 mA/cm^2 for 2 h. The current duration was varied from 2 to 6 h at 0.31 mA/cm^2.

Confocal Laser Scanning Microscopy (CLSM)

The skin with the SC side up was examined using CLSM (Fluoview FV300, Olympus ix70, Olympus, Center Valley, PA). FITC was excited using Argon laser at an excitation wavelength of 488 nm. The images were observed using Plan-neofluor 40/0.85 objective. To analyze the skin distribution of FITC-labeled dendrimers, confocal images were first obtained in the *xy* plane (i.e. parallel to the plane of skin surface). Then the skin surface ($z = 0$) was defined as the imaging plane of brightest fluorescence with a morphology characteristic of the SC surface. To generate the *xz* section, a horizontal line was "drawn" across the region of interest in the $z = 0$ μm-*xy* plane and then optically sliced through the image of successive *xy*-sections to generate *xz*-planar optical cross-sections (Fig. 1). In case of *xyz* images, the skin was scanned from surface ($z = 0\ \mu m$) to 100 μm at a step size of 5 μm/scan. For *xz* sections, the images were optically sectioned from the skin surface ($z = 0\ \mu m$) to 100 μm at a step size of 1 μm/scan. All images were obtained with the same optical aperture, lens and scan speed setting. Blank skin did not show any autofluorescence under the experimental conditions. The images presented are representative of what was observed under different treatment conditions. Each representative image was selected from three to four skin samples, and in each skin three to four different regions were scanned.

Image Analysis

Optical sections (*xyz*) were analyzed using Fluoview software (Olympus, Center Valley, PA). The dendrimer distribution within the confocal images was quantified by integrating the fluorescence pixel intensity (27). Three to four regions were analyzed for each skin. The percent pixels in the SC (0–15 μm) and viable epidermis (VE, 20–100 μm) were calculated using the following formula:

$$\%\ Pixel\ Intensity\ in\ SC = \frac{Total\ Pixel\ intensity\ in\ SC\ (10-15\mu m)}{Total\ Pixel\ Intensity\ in\ skin\ from\ 0-100\mu m}$$

$$\%\ Pixel\ Intensity\ in\ VE = \frac{Total\ Pixel\ intensity\ in\ VE\ (20-100\mu m)}{Total\ Pixel\ Intensity\ in\ skin\ from\ 0-100\mu m}$$

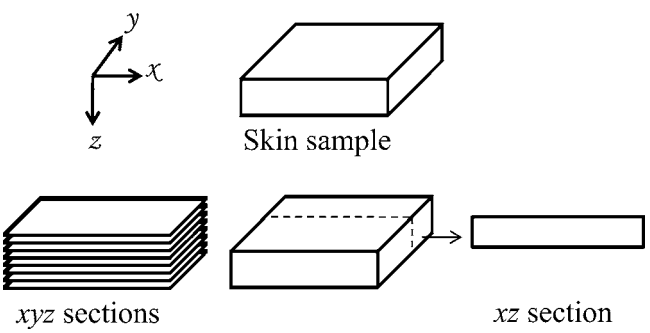

Fig. 1 Schematic representation of confocal optical sections of a skin sample in *xyz* and *xz* planes.

Determination of Dendrimer Amount in Skin Using Spectrofluorimetry

To confirm the results from confocal studies, the amount of FITC-labeled dendrimer in the skin was quantified using spectrofluorimetry. For this study, G_4-NH_2 dendrimer was used. After 2 h of passive or iontophoresis (0.47 mA/cm^2) delivery of G_4-NH_2 dendrimer, the skin was cleaned with water and tape stripped 16–20 times to remove the SC. The tape strips and the remaining skin (epidermis and dermis) were extracted overnight using 30% ethanol. The samples were centrifuged at 10000 rpm for 10 min, and the supernatants were analyzed for fluorescence at ($\lambda_{ex}=490$ nm and $\lambda_{em}=520$ nm) using a spectrofluorimeter (Spectra Max, Molecular devices, Sunnyvale, CA). Skin components did not interfere at the measured wavelength.

Skin Cryosections

The skin sample was cut to a small piece and snap frozen in optimum cutting temperature (OCT, Tissue Tek, Torrance, CA) medium placed in isopentane under liquid nitrogen. The OCT block was then sectioned to 6 μm sections in a cryostat (UV800, Leica Microsystems, Bannockburn, IL). The skin section was collected on glass slides and air dried overnight. Cover slip was placed over the skin section and sealed using cytoseal (Vector laboratories, Burlingame, CA). Upright fluorescence microscope (Olympus AX70, Center Valley, PA) was used for imaging the skin sections. To study the skin morphology, skin section was counterstained with hematoxylin (Vector laboratories, Burlingame, CA) for 30 s and observed under upright light microscope (Olympus AX70, Center Valley, PA). Images were acquired with 10*x* or 20*x* objective lens.

Statistical Analysis

The results are presented as mean ± SD. The differences between various treatment groups were compared using one-way ANOVA (Instat, Graph Pad Software Inc., La Jolla, CA) at $p<0.05$. A confidence interval of 95% was used to test the significant difference between the treatment groups.

RESULTS

Characterization of FITC-Dendrimer Conjugates

Amine-terminated PAMAM dendrimer was covalently linked with FITC through a thiourea bond. On the other hand, the surface of carboxyl-terminated PAMAM dendrimer was modified with ethylenediamine, and the resultant amine group was used to form thiourea bond with FITC (14). Hydroxyl-terminated PAMAM dendrimer was linked to FITC through a thiocarbamate bond (14). The purity of FITC-dendrimer conjugate was confirmed by the absence of spot for free FITC in TLC (data not shown). A similar method has been used in the literature to confirm the purity of FITC-dendrimer conjugates (23). FTIR was used to characterize the FITC-labeled dendrimer conjugates, and the spectra for G_4-NH_2, $G_{3.5}$-COOH and G_4-OH dendrimers are shown in Fig. 2. The formation of the FITC-dendrimer conjugate is evident from the disappearance of the characteristic isothiocyanate stretching band of FITC at 2018 cm^{-1} (28) and appearance of the thiourea/thiocarbamate stretching bands in 1100–1500 cm^{-1}and 400–600 cm^{-1} regions (28,29). Further, the absence of isothiocynate stretching band of FITC at 2018 cm^{-1} confirms the purity of FITC-dendrimer conjugates.

The conjugation of FITC to dendrimer was also confirmed by proton NMR (see Fig. S1, Supplementary Material). UV-visible spectroscopy was used to calculate the number of FITC attached to dendrimer. The λ_{max} for free FITC was 495 nm, while the λ_{max} shifted to 500 nm for dendrimer-FITC conjugate (see Fig. S2, Supplementary Material). About 1–3% of the surface groups were labeled with FITC (Table I). However, in the case of G4-NH_2 dendrimer, 7% of the surface functional groups were labeled with FITC, and in the case of G4-OH 0.2% of the surface groups were labeled with FITC. The results are consistent with the literature where 0.1–9.2% FITC conjugation has been reported for dendrimers (14).

Table I shows the particle size of FITC-labeled dendrimers and their zeta potential. The particle size increased with increase in dendrimer generation. Due to the compact branching architecture of dendrimer and the close arrangement of functional groups, the size increases only by 1–2 nm with increase in dendrimer generation (7). G_4-NH_2 dendrimer had a positive zeta potential which increased with increase in number of surface amine groups. On the other hand, $G_{3.5}$-COOH had a negative zeta potential. The G_4-OH had a low negative zeta potential indicating the weak ionization of the surface hydroxyl groups (25,30). Due to the weak ionization of surface hydroxyl group, it is considered as a relatively neutral dendrimer compared to amine and carboxyl-functionalized dendrimers (14,25). The zeta potential values are comparable to literature values (31); further, at the concentrations used in this study the dendrimers do not aggregate (20).

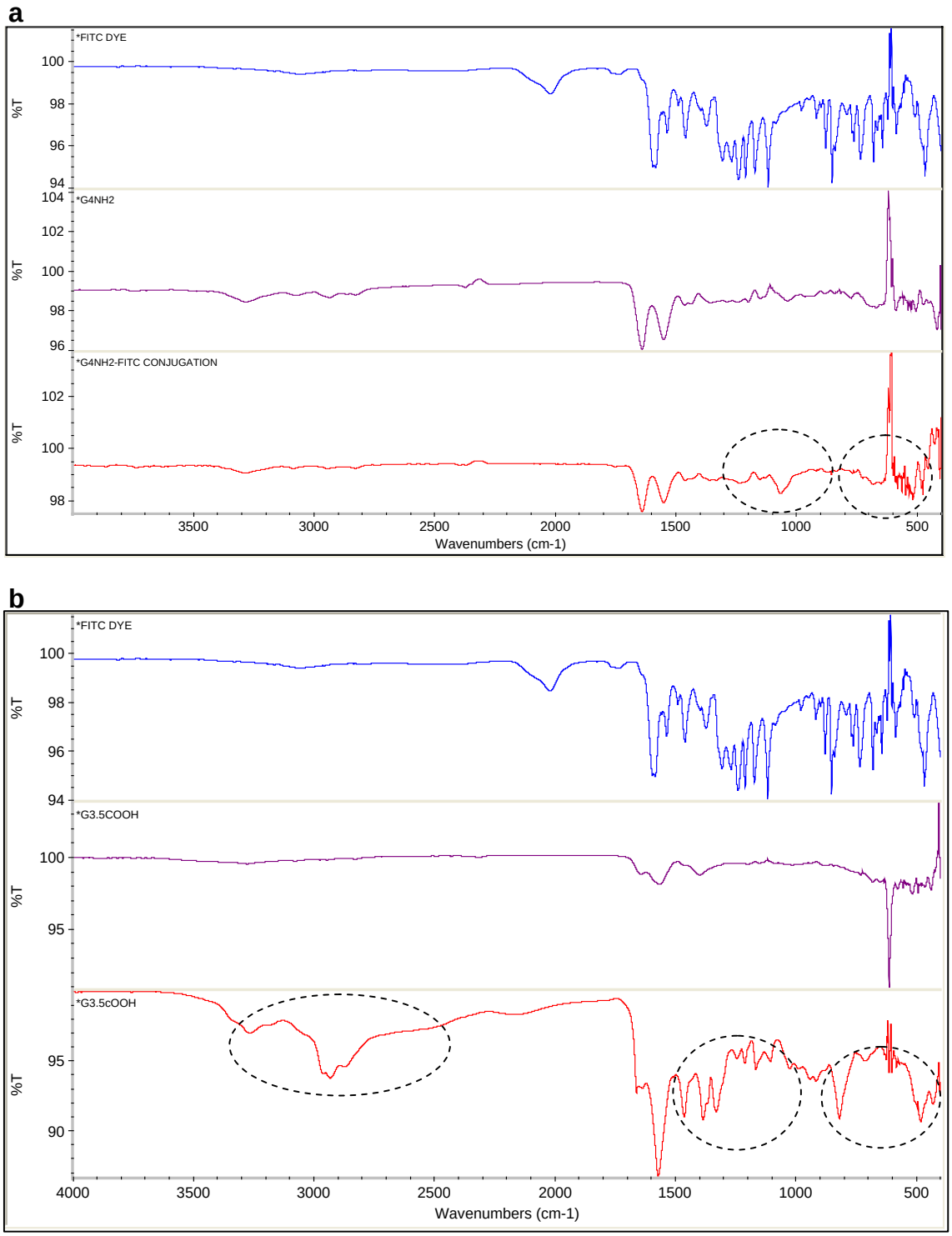

Fig. 2 FTIR spectra of (**a**) FITC-G_4-NH_2 dendrimer conjugate, (**b**) FITC-$G_{3.5}$-COOHdendrimer conjugate and (**c**) FITC-G_4-OHdendrimer conjugate.

Thickness of Stratum Corneum

For determining the depth of skin penetration of dendrimers by CLSM, it is important to know the SC thickness. Therefore, the thickness of porcine SC was determined using tape stripping method. After each tape strip, TEWL increased, but significantly increased after most of the SC (~20 μm) was removed (Fig. 3). The average TEWL value after complete removal of SC was 40 g/m^2/h (Fig. 3). There was some variation in the

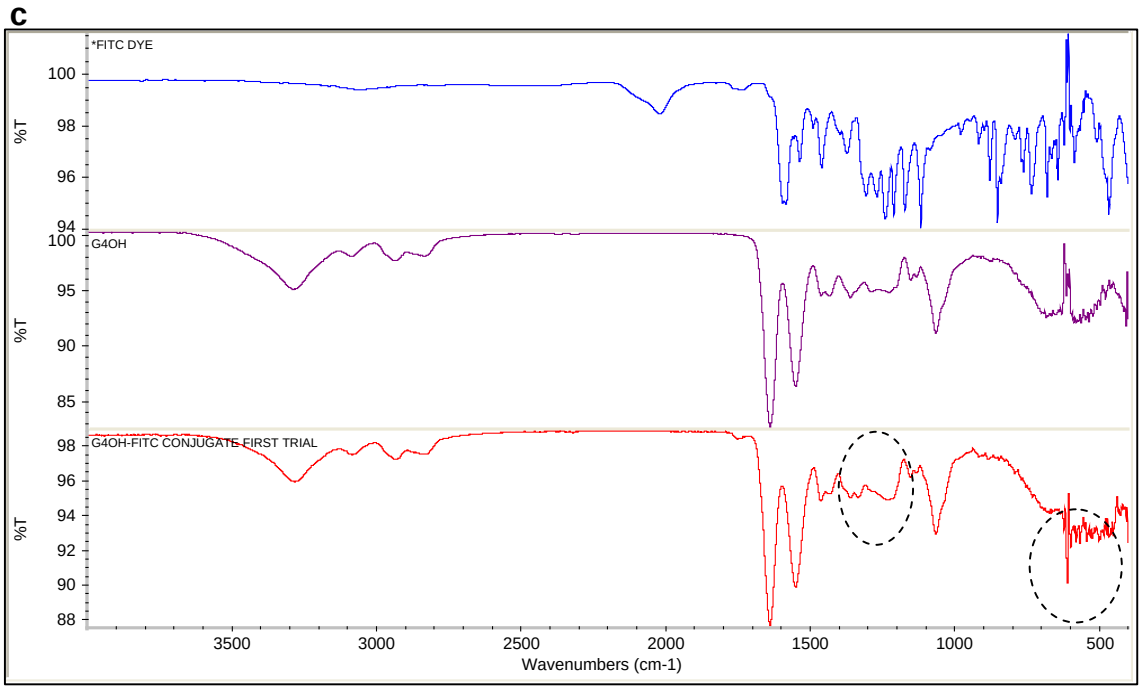

Fig. 2 (continued)

thickness of SC depending on the age of animal and site of ear from where the skin was removed. The number of tape strips required for complete removal of SC was between 15 to 25 strips for the skin samples. However, a significant increase in TEWL was observed at around 20 μm. Therefore, for microscopy studies, the SC thickness was considered to be 20 μm. This is within the reported SC thickness (17–28 μm) for porcine ear skin (22).

Passive Skin Penetration of Dendrimers

The G_4-NH_2, $G_{3.5}$-COOH and G_4-OH dendrimers have 64 surface-functional groups and comparable molecular weight (Table I). Figure 4 shows the CLSM images in *xyz* plane from surface to 100 μm in the skin after treatment with dendrimers. After passive application, dendrimers were mainly limited to SC (Fig. 4). However, G_4-NH_2 dendrimer showed higher penetration into SC compared to $G_{3.5}$-COOH and G_4-OH dendrimers (Fig. 4). Unlike the FITC-dendrimer conjugates, the free FITC was mainly bound to the SC (Fig. 4). We also tape stripped the skin to remove SC and then observed for fluorescence on the surface of tape-stripped skin. As can be seen in Fig. 5, the fluorescence from free FITC was diffuse, while the fluorescence from FITC-G_4-NH_2 dendrimer conjugate was mainly found in the intercellular regions. The results confirm that the FITC label was intact in the dendrimer conjugate.

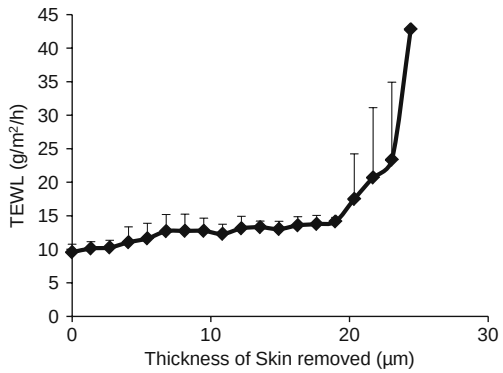

Fig. 3 Transepidermal water loss from porcine skin after tape stripping. Values represent mean of four experiments with standard deviation.

To determine if the dendrimer showed a time-dependent skin penetration, the skin was treated with G_4-NH_2 dendrimer for 12 and 24 h in addition to 2 h treatment. The skin penetration of G_4-NH_2 dendrimer linearly increased with increase in treatment time (Fig 6a). With increasing treatment time, a greater proportion of the dendrimer was found to partition from SC into the viable epidermis (Fig. 6b).

Iontophoretic Skin Penetration of Dendrimers

The *xz* optical sections of skin after passive and iontophoretic (0.31 mA/cm^2) treatment with dendrimers of different surface groups are shown in Fig. 7. After iontophoresis,

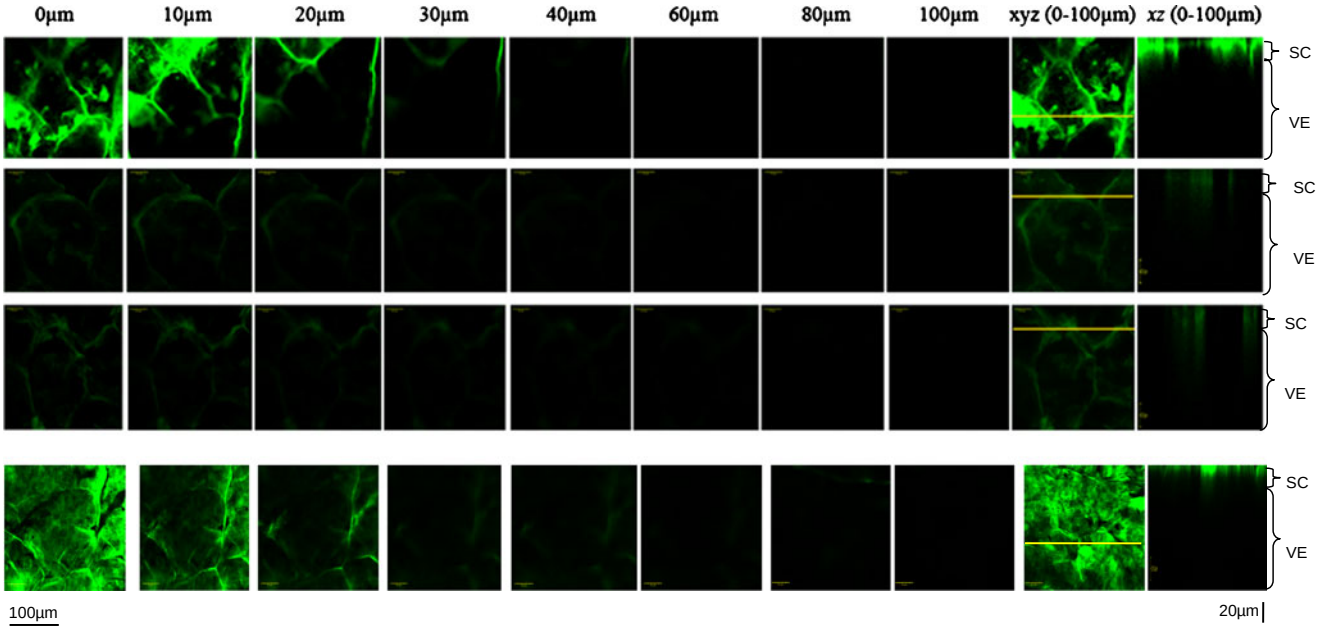

Fig. 4 CLSM images of excised porcine skin after 2-h treatment with FITC-labeled G_4-NH_2, $G_{3.5}$-COOH G_4-OH dendrimers and free FITC (from top to bottom). Images represent sequential scans in *xyz* plane from 0 (skin surface), 10, 20, 30, 40, 60, 80 and 100 μm. Cumulative *xyz* image represent cumulative of all the optical sections from 0–100 μm in *xyz* scan. The *xz* scan from surface to 100 μm in skin was taken at the position of line drawn on the *xyz* cumulative image. Images are representative of at least three experiments.

cationic dendrimer penetrated into the skin to a depth of 80 μm, while fluorescence was found up to a depth of 40 μm and 60 μm for anionic and neutral dendrimers, respectively. Figure 8 shows the percent of total pixels present in viable epidermis (20–100 μm) after 2 h of passive and current application, respectively. Iontophoresis significantly ($p<0.05$) enhanced the skin penetration of cationic and neutral dendrimers into viable epidermis. Iontophoresis increased the dendrimer penetration into viable epidermis by 2.5-fold. In the case of anionic dendrimer, there was no significant difference in skin penetration between cathodal iontophoresis and passive delivery (Fig. 8). Similarly, anodal iontophoresis also did not enhance the skin penetration of anionic dendrimer (data not shown). It is important to note that for G_4-NH_2 dendrimer, 2 h of iontophoresis resulted in a comparable skin penetration to 12 h of passive delivery (i.e. ~20% of dendrimer penetrated into viable epidermis). However, no dendrimer was detected in the receptor phase for any of the dendrimers used in this study when measured by spectrofluorimetry.

To confirm the results from confocal microscopy studies, the amount of FITC-labeled G_4-NH_2 dendrimer in skin was quantified using spectrofluorimetry. After 2 h of passive and iontophoretic application, the amount of FITC-dendrimer in the SC and viable epidermis/dermis is shown in Fig. 9. There was no significant difference in the amount

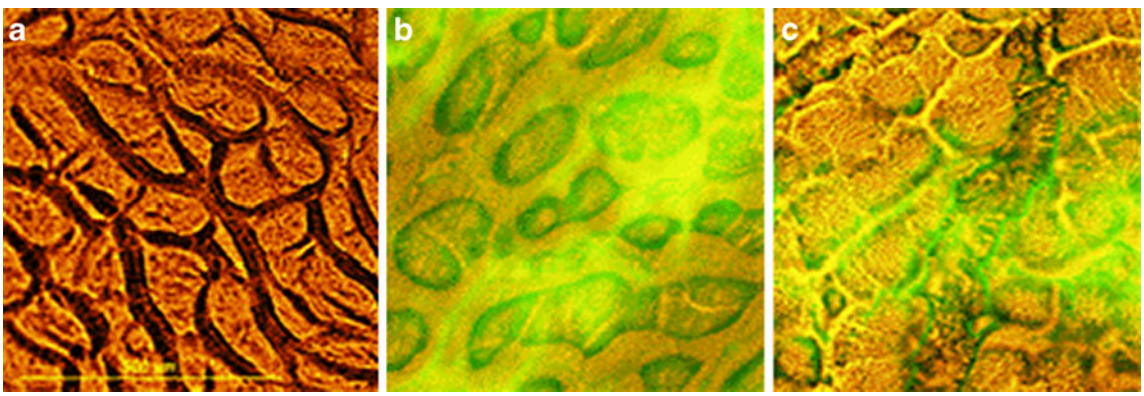

Fig. 5 Fluorescence microscopy images of tapestripped skin for (**a**) blank, (**b**) after treatment with free FITC and (**c**) after treatment with FITC-labeled G_4-NH_2 dendrimer for 2 h.

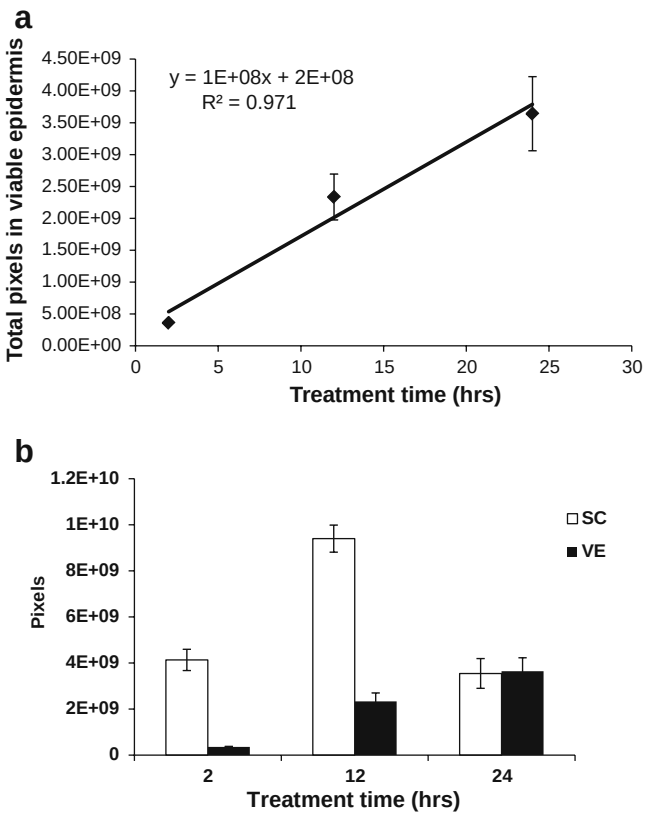

Fig. 6 (**a**) Total integrated pixels in the viable epidermis (20–100 μm) for CLSM optical sections after passive treatment with G_4-NH_2dendrimer for 2-24 hrs. (**b**) Fluorescence pixels in stratum corneum (SC 0–15 μm) and viable epidermis (VE from 20–100 μm) after treating porcine skin with G_4-NH_2dendrimer for 2-24 hrs. Values represent mean ± SD ($n=4$).

of dendrimer in SC, but the amount of dendrimer in the viable epidermis was 3-fold higher ($p<0.05$) after iontophoretic delivery of dendrimer. In terms of percent amount of dendrimer in the viable skin layers, the penetration enhancement (data not shown) was comparable to the enhancement calculated from the percent pixels in confocal microscopy studies (2-fold).

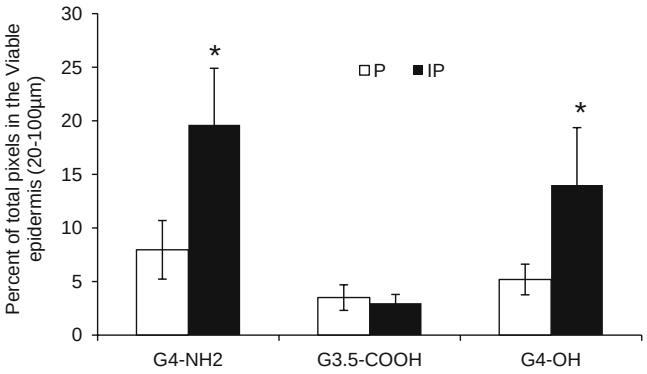

Fig. 8 Percent pixels in viable skin (20–100 μm) after passive and iontophoretic treatment (2 h; 0.31 mA/cm^2) with different dendrimers. P—passive application; IP—iontophoresis application. Y-axis represents percent of the total pixels (0–100 μm) in viable epidermis (20–100 μm). Values represent mean ± SD ($n=4$). * represents that the value is significant at $p<0.05$ compared to respective treatments.

Influence of Current Strength and Current Duration

The G_4-NH_2 which showed higher skin penetration was used to study the influence of current strength and current duration on iontophoretic transport of dendrimers. An increase in current strength significantly ($p<0.05$) enhanced the skin penetration of dendrimer (Fig. 10a). Increase in current strength from 0.31 mA/cm^2 to 0.47 mA/cm^2 increased the skin penetration of dendrimer by 3-fold.

When the current application time was increased, the skin penetration of dendrimer increased (Fig. 10b). However, there was no significant increase in fluorescence in SC with increase in current application time. On the other hand, an increase in current application time from 2 to 4 h enhanced the dendrimer penetration into viable epidermis by 3-fold; 6 h current application was not significantly ($p>0.05$) different from 4 h of current application.

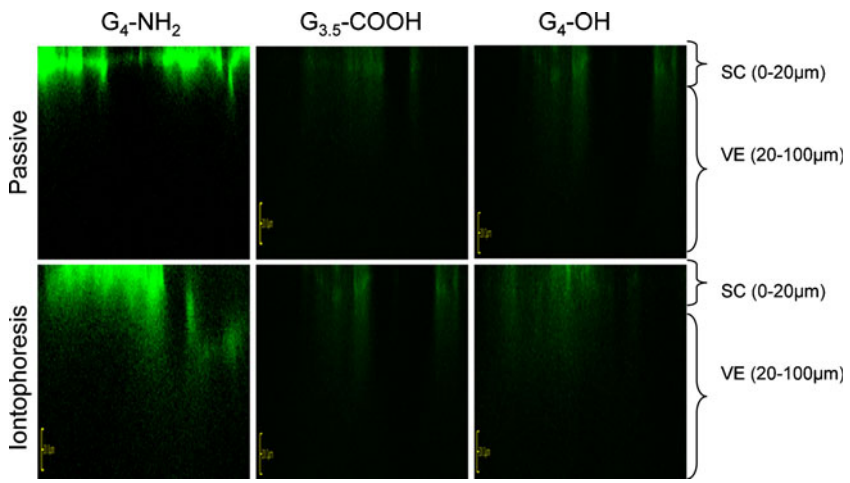

Fig. 7 CLSM images of porcine skin after 2 h of passive and iontophoresis (0.31 mA/cm^2) application. Images were taken in *xz* plane from surface to 100 μm in skin. The vertical bar represents 20 μm. SC—stratum corneum (0–20 μm); VE—viable epidermises (20–100 μm). The images are representative of three experiments.

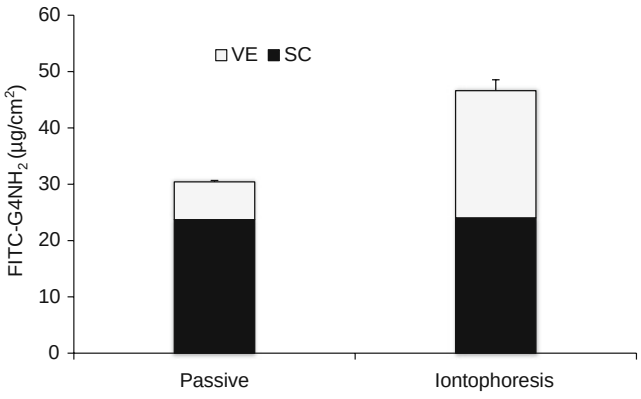

Fig. 9 Amount of FITC labeled G_4-NH_2 dendrimer in stratum corneum (SC) and epidermis/dermis (VE) after passive and iontophoretic (0.31 mA/cm^2) delivery for 2 h. Values represent mean ± SD ($n = 4$).

Skin Transport Pathways for Dendrimer

To determine the transport pathways, the surface confocal images were recorded (Fig. 11). With passive delivery, the cationic dendrimer was mainly distributed in the skin furrows, the intercellular regions, and the hair follicles (Fig. 11a-c). A strong fluorescence was found on the skin surface in presence of iontophoresis (Fig. 11f). In the case of iontophoresis, dendrimers were also found in the skin furrows, intercellular lipid regions and hair follicles (Fig. 11d-f). However, it was observed that there were clustered regions of bright fluorescence in the iontophoresis treatment group (Fig. 11d). These regions were repeatedly observed only in the iontophoretic treatment group which appears to be localized transport regions for the dendrimer.

Hematoxylin-stained skin cryosections after passive and iontophoresis application of G_4-NH_2 dendrimer were used to study the changes in skin morphology. Figure 12 shows that the skin morphology was not grossly altered after dendrimer and/or current application and was similar to control skin. Further, to confirm the CLSM results, the distribution of FITC-labeled dendrimer in skin cryosections was also studied. Figure 13 shows the bright field and fluorescence images from skin cryosections after G_4-NH_2 dendrimer treatment. The depth of penetration of G_4-NH_2 dendrimer observed from skin cryosections was similar to that seen in the CLSM studies. Fluorescence images from the skin cryosections after passive treatment with G_4-NH_2 dendrimer showed fluorescence only in the SC (Fig. 13). On the other hand, in the case of iontophoresis, the fluorescence was observed in viable epidermis and even in the upper dermis layer (Fig. 13).

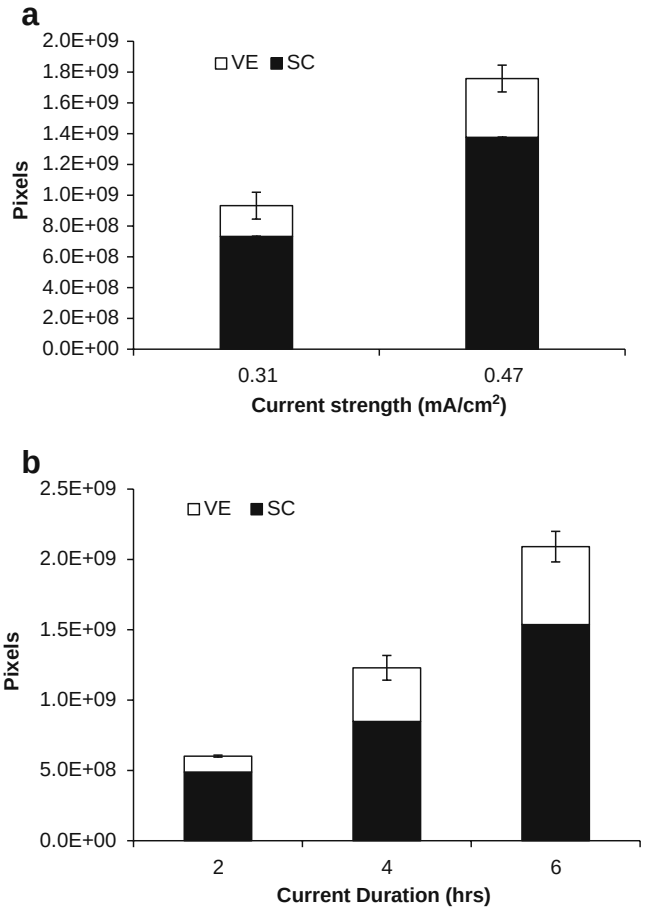

Fig. 10 Influence of current strength (**a**) and current application time (**b**) on skin penetration of FITC-labeled G_4-NH_2 dendrimer in stratum corneum (SC) and viable epidermis (VE). Values represent mean ± SD ($n = 4$). The y-axis represents the pixels determined from CLSM.

Influence of Generation on Skin Penetration of Cationic Dendrimers

Since cationic dendrimer showed higher skin affinity, the effect of molecular weight and charge density on skin penetration were studied using G_2-NH_2 to G_6-NH_2 cationic dendrimers. Figure 14 shows the percent fluorescence pixels as a function of molecular weight of dendrimers. The extent of skin penetration of dendrimers exponentially decreased with an increase in molecular weight of dendrimers. In the case of passive delivery, most (>60%) of the dendrimer was found in the SC for dendrimer generations >G_2-NH_2 (data not shown). Compared to passive delivery, the decrease in skin penetration of dendrimers with increase in dendrimer generation was less steep after iontophoresis (Fig. 14). The penetration enhancement for higher generation dendrimers (G_4-NH_2 to G_6-NH_2) was two-fold, while in the case of lower generation dendrimers (G_2-NH_2 and G_3-NH_2) there was only a slight increase in penetration enhancement. The results indicate that iontophoresis can be used to increase the skin penetration of higher generation dendrimers compared to lower generation dendrimers.

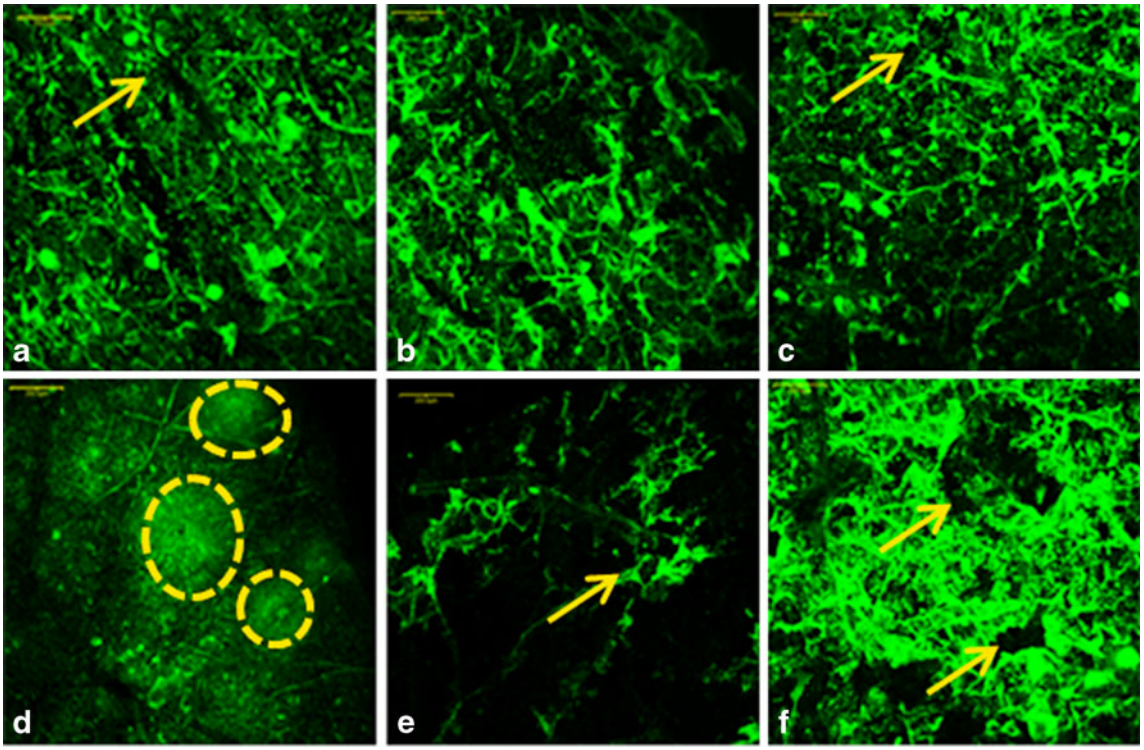

Fig. 11 CLSM images of excised porcine skin after 2 h of passive (a, b and c) and 0.31 mA/cm^2 current application (d, e and f) with G_4-NH_2 dendrimer. Images represent the skin surface in *xy* plane under 4*x* objective. The dotted circles represent the localized regions of high fluorescence and arrows show hair follicles. The images a, b and c show different regions in the skin after passive transport of dendrimers including the intercellular lipid region and hair follicles (*arrows*). The images d, e and f show different regions of the skin after iontophoretic transport of dendrimer. The iontophoretic transport regions include skin furrows, highly localized intracellular transport region (*dotted circle*), intercellular lipid regions and hair follicles (*arrows*).

DISCUSSION

Dendrimers are branched polymers that can undergo multivalent interactions due to the high density of surface-functional groups (8,9). Although dendrimer transport has been studied across several biological membranes (10–13,16), its transport through skin has not been characterized. For transcutaneous drug delivery, the carrier should cross the SC barrier to deliver the drug to the underlying epidermis and dermis. Findings from this study provide preliminary understanding on the influence of physicochemical properties of dendrimers on their skin penetration. CLSM offers the advantage of directly examining the distribution of fluorescent molecules at multiple depths in the skin without mechanical sectioning or fixing the skin (32). Therefore, CLSM can be used to understand the relative penetration of molecules. However, it is difficult to relate the fluorescence intensity of CLSM images directly to the concentration of fluorophore due to signal attenuation from deeper skin layers (32). We validated the use of CLSM for determining the relative skin penetration of dendrimers by comparing the results with the quantitative estimation of dendrimer-FITC by spectrofluorimetry. Although the amounts of FITC-dendrimer determined between both methods were different, the extent of penetration enhancement was comparable. Unlike the CLSM where the fluorescence was measured only up to 100 μm deep from the skin surface, the whole viable epidermis/dermis was

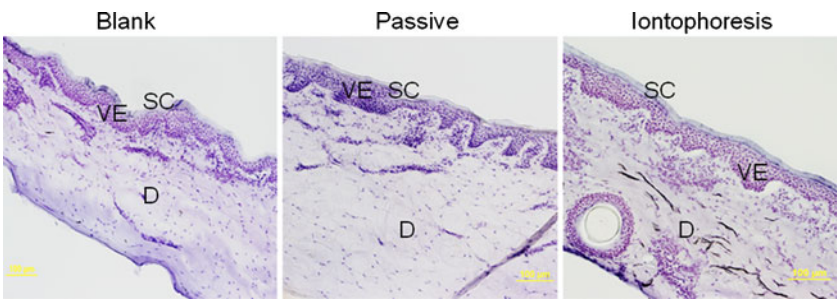

Fig. 12 Hematoxylin stained cryosections of control skin, after 2 h of passive and iontophoretic delivery of G_4-NH_2 dendrimer. Images were taken using 10*x* objective. SC—stratum corneum; VE—viable epidermis; D—dermis.

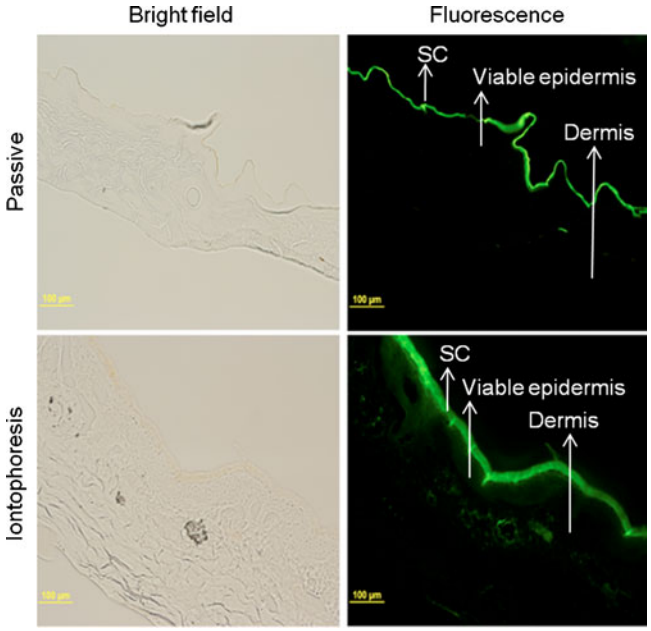

Fig. 13 Fluorescence microscopic images of cyrosections of porcine ear skin after 2 h of passive (*upper panel*) and iontophoretic delivery (*lower panel*) of G_4-NH_2 dendrimer. Corresponding bright field images are shown in the left panel. Images were taken using 10*x* objective.

used for the spectrofluorimetry estimation, and this could lead to differences in the absolute quantities determined by the two methods. However, since our goal was to measure the ability of dendrimers to cross the SC, CLSM can provide a reasonable semi-quantitative estimation of skin transport (27,32,33). Turner *et al.* (27) studied the extent and distribution of iontophoretic transport of FITC-labeled poly-L-lysines (PLL) in hairless mouse skin. Quantitative analysis of CLSM images was used to estimate the contribution of follicular and non-follicular pathways to iontophoretic transport of PLL. Similarly, Brus *et al.* (34) have used CLSM to characterize and quantify the skin

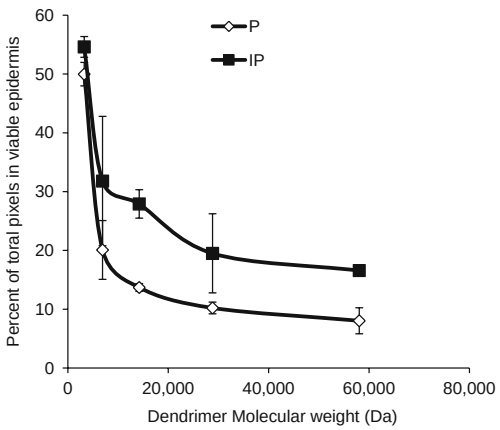

Fig. 14 The influence of molecular weight dendrimer (G_2-NH_2 to G_6-NH_2) penetration into viable epidermis in absence (Passive; P) and presence of iontophoresis (IP). Values represent mean ± SD ($n = 4$).

penetration of oligonucleotide-polyethylene imine complex by iontophoresis.

The isoelectric point of skin is 4 to 5, and at physiological pH, the skin is negatively charged (35). Therefore, cationic molecules have intrinsic affinity for negatively charged skin membrane (27,36). In a recent study by Wu *et al.*, (37), amine-functionalized (cationic) polystyrene nanoparticles were found to be highly concentrated in the SC compared to the carboxyl-functionalized (anionic) polystyrene nanoparticles. The higher skin affinity of cationic dendrimers is consistent with the dendrimer penetration through other biological membranes (10,38). The higher skin penetration of cationic dendrimers is due to their binding to the negatively charged skin (19,20). Earlier, we have reported that cationic dendrimers caused higher skin penetration enhancement of 5-fluorouracil (5FU) compared to neutral and anionic dendrimers (20). The cationic dendrimers increased the skin penetration of 5FU by mainly interacting with the skin lipids (20). Due to the large molecular weight (G_4-NH_2 has an Mwt of 14.5 kDa), the skin penetration of dendrimer is slow and increases with increase in treatment time. This is evident from Fig. 6b, where an increase in treatment time led to a higher dendrimer partitioning from SC to viable skin. In our earlier studies, we found that the flux of 5FU was proportional to the length of skin pre-treatment time (2–24 h) with G_4-NH_2 dendrimer (19). More importantly, the penetration enhancement was directly related to the percent decrease in skin resistance ($r^2 = 0.995$). The TEWL and skin resistance did not significantly change after 2 h of pre-treatment with G_4-NH_2 dendrimer, while 12 and 24 h treatment caused a significant change in TEWL and skin resistance (19). This suggests that the cationic dendrimers penetrate the skin by interacting with the intercellular lipids, which was also evident from the localization of FITC-dendrimer in the intercellular lipid regions (Figs. 5 and 11). Further studies using model skin lipids are required to understand these interactions.

Iontophoresis has been used to enhance the skin penetration of charged molecules and neutral molecules (21). In the case of small charged molecules, iontophoresis increases skin penetration mainly by electrorepulsion, i.e when a cation is delivered from anode and when an anion is delivered from the cathode (21). Due to the permselectivity of skin to cations, the solvent flow during iontophoresis is from anode to cathode at physiological pH (39). Therefore, in case of anodal iontophoresis, the transport of a positively charged molecule benefits from electroosmosis in addition to electrorepulsion. Neutral molecules are predominantly transported by electroosmosis when delivered from the anode (21). Unlike small molecules, the macromolecules are mainly transported by electroosmosis, (40). The skin penetration of cationic dendrimer after 2 h of

iontophoresis showed similar skin penetration to 12 h of passive delivery, which implies that dendrimer can deliver the drug payload in a shorter period by iontophoresis. Since G_4-OH dendrimer has a weak negative charge, it is generally considered to be neutral at physiological pH (14, 25). Therefore, G_4-OH dendrimer is mainly expected to be transported by electroosmosis. Ruddy and Hadzija (41) reported that the polyethylene glycols are transported by electroosmosis during iontophoresis. Since it is difficult to deliver a highly negatively charged macromolecule through the negatively charged skin by electrorepulsion, there was no penetration enhancement for $G_{3.5}$-COOH dendrimer. Furthermore, during cathodal iontophoresis, the electroosmotic flow is in the negative direction to the transport of anionic dendrimer (39). When the anionic dendrimer was delivered from the anode, still there was no penetration enhancement (data not shown). On the other hand, in the literature, the skin penetration of large anions is reported to be enhanced by electroosmosis using anodal iontophoresis (42). It is important to note that most of the iontophoretic studies reported in the literature are for linear macromolecules (42). In contrast, branched architecture and high charge density in dendrimers may lead to differences in the electroosomotic transport through the skin pores. However, further studies are required to understand the relative contribution of electrorepulsion and electroosmosis to iontophoretic transport of dendrimers.

The iontophoretic transport can be controlled by altering the current strength and/or duration of current application. An increase in current strength, as expected, led to increase in skin penetration of dendrimers. Similarly, the increase in duration of current application also led to increase in skin penetration. However, when the current was applied continuously for >4 h, there was minimal increase in skin penetration of dendrimers. The continuous application of current for a prolonged period causes electrochemical polarization and accumulation of charge on the skin, leading to reduced transport efficiency (43). Furthermore, in the case of multivalent macromolecules, the iontophoretic transport pathways may get saturated on prolonged current application (33,44,45). On the other hand, the increased binding of cationic dendrimers to SC can neutralize the negative charge of skin, leading to attenuation of electroosmotic flow from anode to cathode (46), resulting in decreased transport efficiency.

In general, the skin penetration decreases with increasing molecular weight of the permeant (47). Similar to the results from this study, the dendrimer penetration was inversely related to molecular weight in other biological membranes (10,16). Iontophoretic transport of FITC-labeled PLL (4–26 kDa) was inversely related to the molecular weight of PLL (27). With an increase in dendrimer generation, the molecular weight doubles (Table I). Further, the number of surface-functional groups also doubles, i.e. the amine group increases from 16 to 256 from G2 to G6-NH_2 dendrimer (Table I). The increase in charge density can increase the binding of dendrimers to the negatively charged SC, resulting in lesser penetration into the viable epidermis. Venuganti and Perumal (20) reported that the extent of skin penetration enhancement of 5FU was inversely related to the molecular weight of cationic dendrimers. Similarly, the extent of interaction of dendrimers with the intercellular skin lipids was inversely related to the dendrimer generation (20). The decrease in skin resistance was in the following order G2-NH_2 > G4-NH_2 > G6-NH_2 dendrimer (20). Since the lower generation dendrimer has a lower molecular weight, it has higher passive penetration than the higher generation dendrimers; therefore, iontophoresis resulted in relatively lesser skin penetration enhancement compared to the higher generation dendrimers. On the other hand, the higher charge density in the higher generation dendrimers is expected to increase the electromigration of dendrimers (48). However, this does not seem to be the case, and electroosmosis appears to be a major transport mechanism of dendrimers. This is evidenced by the fact that the penetration enhancement was similar for the higher generation dendrimers (G5-G6 NH_2). These two dendrimers also had very similar zeta potential (Table I). Unlike electrorepulsion, which decreases sharply with increasing molecular weight, the electroosmosis remains relatively constant for macromolecules (40). The difference in surface charge density may play a significant role in skin transport of dendrimers than the hydrodynamic radius. The dendrimer size changes by only 1–2 nm as opposed to increase in surface-functional groups, which doubles with every dendrimer generation (7). This is also reflected in the size and zeta potential values in Table I. As stated earlier, the increased binding of higher generation cationic dendrimers to SC can neutralize the negative charge of skin, leading to attenuation of electroosmotic flow from anode to cathode (46), resulting in decreased penetration enhancement. However, further studies are required to understand the role of electroosomosis in iontophoretic transport of dendrimers.

Dendrimer is transported through similar skin transport pathways (appendageal and intercellular lipid pathways) as liposomes and polymeric nanoparticles (6,37,49). In presence of iontophoresis, PLL has been reported to penetrate through both intercellular lipid pathways and hair follicles in hairless mouse skin (27). However, PLL was mainly found to bind to the lipid bilayers in the intercellular pathway (27). In our study, the dendrimers were found to be transported through similar pathways during iontophoresis. However, we observed localized regions of transport that were not associated with appendages. These regions

may represent areas where local skin resistance is lower than adjacent areas (50). Further studies are required to characterize these localized transport regions. It is unlikely that FITC is detached from the dendrimer in skin. As opposed to the FITC-dendrimer conjugate, free FITC was found to be homogenously distributed on the skin surface (Fig. 5). Furthermore, the dendrimer is non-biodegradable. Studies with other FITC-conjugated non-degradable polymers through similar type of covalent bond have been reported to be stable in the skin (27,49). It is possible that the difference in the skin penetration of dendrimers may be influenced by the difference in the FITC labeling. Considering that number of FITC molecules is relatively small compared to the large number of surface-functional groups in dendrimers, this difference will likely have lesser impact on skin penetration. This is supported from similar zeta potential for FITC-labeled dendrimers and unlabeled dendrimers (data not shown).

Overall, the results from this study demonstrate that dendrimers can be used as nanocarriers for drug delivery to skin for various skin conditions. The unique advantage of dendrimer as a nanocarrier is the ease with which the number and type of surface-functional groups can be altered (7) to target the drugs to specific layer in the skin. The drugs can be complexed to the surface-functional groups or trapped inside the dendrimer core (7,8). Further, the drugs can also be conjugated to the surface-functional groups to retain the drug in skin and minimize systemic absorption. For example, sunscreens can be conjugated to higher generation dendrimer such as G5 or G6 dendrimer to retain the sunscreen on the skin surface for maximal sun protection and at the same time minimize systemic absorption.

In general, charged molecules are suitable for iontophoretic transport. Therefore, the dendrimers can be used as charged carriers for iontophoretic delivery of drugs which do not have any charge. Cationic dendrimers are promising transfecting agents (17), and they can be used as delivery carriers for oligonculeotides siRNA or DNA. The skin penetration of these negatively charged molecules is generally poor but can be increased by complexing it with cationic dendrimers and delivering the charged nanocomplexes into the skin using iontophoresis (34). These nanocomplexes, in addition to aiding skin transport, will also help in enhancing the cell uptake of anti-sense oligonucleotides and DNA (17). We have used this approach to deliver Bcl-2 anti-sense oligonucleotide for treating skin cancer in mice (unpublished results). Similar approaches can be extended to other skin diseases. Due to the multiple surface functional groups, the dendrimers can also be used for simultaneously delivering multiple drugs to skin by iontophoresis.

CONCLUSIONS

The results from the study show that dendrimers penetrate the skin in a charge- and molecular-weight-dependent manner. Cationic dendrimers have a higher skin affinity than neutral and anionic dendrimers. The skin penetration of cationic dendrimers increased with increase in treatment time. Iontophoresis increased the skin penetration of cationic and neutral dendrimers into viable epidermis. The skin penetration of cationic dendrimers is inversely related to the dendrimer molecular weight. Drugs can be complexed or conjugated to the dendrimers for maximizing the drug concentration in the skin and minimizing the systemic absorption. Further, in the case of negatively charged macromolecules, such as DNA, oligonucleotides and siRNA, they can be complexed with cationic dendrimers, and the charged dendriplexes can then be topically delivered using iontophoresis.

ACKNOWLEDGMENTS

We thank Dr. Kelly Bruns and Mr. Adam Rhody, Meat Science Department, SDSU for providing porcine skin.This work was supported by South Dakota Governor Round's 2010 individual research seed grant and Department of Pharmaceutical Sciences, South Dakota State University.

REFERENCES

1. Scheuplein RJ, Blank IH. Permeability of the skin. Physiol Rev. 1971;51:702–47.
2. Downing DT. Lipid and protein structure in the permeability barrier of mammalian epidermis. J Lipid Res. 1992;33:301–13.
3. Naik A, Kalia YN, Guy RH. Trbansdermal drug delivery: overcoming skin's barrier function. Pharm Sci Technol Today. 2000;3:318–26.
4. Prausnitz MR, Mitragotri S, Langer R. Current status and future potential of transdermal drug delivery. Nat Rev Drug Discov. 2004;3:115–24.
5. Venuganti VK, Perumal OP. Nanosystems for dermal and transdermal drug delivery. In: Pathak Y, Thassu D, editors. Nanoparticulate drug delivery systems: formulation and characterization. New York: Informa Health; 2009. p. 124–53.
6. Cevc G, Vierl U. Nanotechnology and the transdermal route: a state of the art review and critical appraisal. J Control Release. 2010;141:277–99.
7. Esfand R, Tomalia DA. Poly (amidoamine) (PAMAM) dendrimers: From biomimicry to drug delivery and biomedical applications. Drug Discov Today. 2001;6:427–36.
8. Kannan RM, Perumal O, Kannan S. Dendrimers and hyperbranched polymers in drug delivery. In: Labhateswar V, Pelecky L, editors. Biomedical applications of nanotechnology. New Jersey: Wiley; 2005. p. 105–30.
9. Mammen M, Choi SK, Whitesides GM. Polyvalent interactions in biological systems: implications for design and use of multivalent ligands and inhibitors. Angew Chem Int Ed. 1998;37:2754–94.

10. El-Sayed M, Ginski M, Rhodes C, Ghandehari H. Transepithelial transport of poly (amidoamine) dendrimers across Caco-2 cell monolayers. J Control Release. 2002;81:355–65.
11. Bai S, Ahsan F. Synthesis and evaluation of pegylated dendrimeric nanocarrier for pulmonary delivery of low molecular weight heparin. Pharm Res. 2009;26:539–48.
12. Vandamme TF, Brobeck L. Poly(amidoamine) dendrimers as ophthalmic vehicles for ocular delivery of pilocarpine nitrate and tropicamide. J Control Release. 2005;102:23–38.
13. Menjoge AR, Navath RS, Asad A, Kannan S, Kim CJ. Transport and biodistribution of dendrimers across human fetal membrane: implications for intravaginal administration of dendrimer-drug conjugates. Biomaterials. 2010;31:5007–21.
14. Kitchens KM, Kolhatkar RB, Swaan PW, Eddington NW, Ghandehari H. Transport of poly (amidoamine) dendrimers across caco-2 cell monolayers: influence of size, charge and fluorescent labeling. Pharm Res. 2006;23:2818–26.
15. Malik N, Wiwattanapatapee R, Klopsch R, Lorenz K, Frey H, Weener JW, *et al.* Dendrimers: Relationship between structure and biocompatibility *in vitro*, and preliminary studies on the biodistribution of ^{125}I-labeled polyamidoamine dendrimers in vivo. J Control Release. 2000;65:133–48.
16. El-Sayed M, Kiani MF, Naimark MD, Hikal AH, Ghandehari H. Extravasation of poly(amidoamine) (PAMAM) dendrimer across microvascular network endothelium. Pharm Res. 2001;18:23–8.
17. Dufe's C, Uchegbu IF, Schatzlein AG. Dendrimers in gene delivery. Adv Drug Deliv Rev. 2005;57:2177–202.
18. Chauhan AS, Sridevi S, Chalasani KB, Jain AK, Jain SK, Jain NK, *et al.* Dendrimer mediated transdermal delivery: Enhanced bioavailability of indomethacin. J Control Release. 2003;90:335–43.
19. Venuganti VK, Perumal OP. Effect of poly(amidoamine) PAMAM dendrimer on the skin permeation of 5-fluorouracil. Int J Pharm. 2008;361:230–8.
20. Venuganti VK, Perumal OP. Poly(amidoamine) dendrimers as skin penetration enhancers: Influence of charge, generation and concentration. J Pharm Sci. 2009;98:2345–56.
21. Kalia YN, Naik A, Garrison J, Guy RH. Iontophoretic drug delivery. Adv Drug Deliv Rev. 2004;56:619–58.
22. Jacobi U, Kaiser M, Toll R, Mangelsdorf S, Audring H, Otberg N, *et al.* Porcine ear skin, an *in vitro* model for human skin. Skin Res Technol. 2007;31:19–24.
23. Jevprasesphant R, Penny J, Attwood D, McKeown NB, D'Emanuele A. Engineering of dendrimer surfaces to enhance transepithelial transport and reduce cytotoxicity. Pharm Res. 2003;20:1543–50.
24. Kalia YN, Pirot F, Guy RH. Homogeneous transport in a heterogeneous membrane: water diffusion across human stratum corneum *in vivo*. Biophysical J. 1996;71:2692–700.
25. Diallo MS, Christie S, Swaminathan P, Balogh L, Shi X, Um W, *et al.* Dendritic chelating agents. 1. Cu(II) binding to ethylenediamine core poly(amidoamine) dendrimers in aqueous solutions. Langmuir. 2004;20:2640–51.
26. Rastogi SK, Singh J. Lipid extraction and transport of hydrophilic solutes through porcine epidermis. Int J Pharm. 2001;225:75–82.
27. Turner NG, Ferry L, Price M, Cullander C, Guy RH. Iontophoresis of poly-L-lysines: The role of molecular weight? Pharm Res. 1997;14:1322–133.
28. Do JH, Joun YS, Chung DJ. Cellular-uptake behavior of polymer nanoparticles into consideration of biosafety. Macromol Res. 2008;16:695–703.
29. Oh J, Choi S, Lee G, Kim J, Choy J. Inorganic metal hydroxide nanoparticles for targeted cellular uptake through clathrin mediated endocytosis. Chem Asian J. 2009;4:67–73.
30. Lee JH, Lim Y, Choi S, Lee Y, Kim T, Kim HJ, *et al.* Polyplexes assembled with internally quartnized PAMAM-OH dendrimer and plasmid DNA have a neutral surface charge and gene delivery potency. Bioconjugate Chem. 2003;14:1214–21.
31. Nuha P, Davoren M, Lyng FM, Byrne HJ. Reactive oxygen species induced cytokine production and cytotoxicity of PAMAM dendrimers in J774a.1 cells. Toxicol Appl Pharmacol. 2010;246:91–9.
32. Alvarez-Roman R, Naik A, Kalia YN, Fessi H, Guy RH. Visualization of skin penetration using confocal laser scanning microscopy. Eur J Pharm Biopharm. 2004;58:301–16.
33. Dubey S, Kalia YN. Non-invasive iontophoretic delivery of enzymatically active ribonuclease A (13.6 kDa) across intact porcine and human skins. J Control Release. 2010;145:203–9.
34. Brus C, Santi P, Colombo P, Kissel T. Distribution and quantification of polyethyleneimine oligodeoxyneclotide complexes in human skin after iontophoretic delivery using confocal scanning laser microscopy. J Control Release. 2002;84:171–81.
35. Burnette RR, Ongpipattanakul B. Characterization of the permselective properties of excised human skin during iontophoresis. J Pharm Sci. 1987;76:765–73.
36. Schuetz YB, Carrupt PA, Naik A, Guy RH, Kalia YN. Structure-permeation relationships for the non-invasive transdermal delivery of cationic peptides by iontophoresis. Eur J Pharm Sci. 2006;29:53–9.
37. Wu X, Landfester K, Musyanovych A, Guy RH. Disposition of charged nanoparticles after their topical application to the skin. Skin Pharmacol Physiol. 2010;23:117–23.
38. Perumal OP, Inapagolla R, Kannan S, Kannan RM. The effect of surface functionality on cellular trafficking of dendrimers. Biomaterials. 2008;29:3469–76.
39. Marro D, Guy RH, Delgado-Charro MB. Characterization of the iontophoretic permselectivity properties of human and pig skin. J Control Release. 2001;70:213–7.
40. Guy RH, Kalia YN, Delgado-Charro MB, Merino V, Lopez A, Marro D. Iontophoresis: electrorepulsion and electroosmosis. J Control Release. 2000;64:129–32.
41. Ruddy SB, Hadzija BW. Iontophoretic permeability of polyethylene glycols through hairless rat skin: application of hydrodynamic theory for hindered transport through liquid-filled pores. Drug Des Discov. 1992;8:207–24.
42. Pikal MJ, Shah S. Transport mechanisms in iontophoresis. III. An experimental study of the contributions of electroosmotic flow and permeability change in transport of low and high molecular weight solutes. Pharm Res. 1990;7:222–9.
43. Pillai O, Kumar N, Dey CS, Borkute, Sivaprasad N, Panchagnula R. Transdermal iontophoresis of insulin: III. Influence of electronic parameters. Methods Find Exp Clin Pharmacol. 2004;26:399–408.
44. Cazares-Delgadillo J, Naik A, Ganem-Rondero A, Quintanar-Guerrero D, Kalia YN. Transdermal delivery of cytochrome-c, a 12–4 kDa protein across intact skin by constant current iontophoresis. Pharm Res. 2007;24:1360–8.
45. Kasting GB, Keister JC. Applications of electrodiffusion theory for a homogenous membrane to iontophoretic transport through skin. J Control Release. 1989;8:195–210.
46. Hirvonen J, Guy RH. Transdermal iontophoresis: modulation of electroosmosis by polypeptides. J Control Release. 1998;50:283–9.
47. Potts RO, Guy RH. Predicting skin permeability. Pharm Res. 1992;9:663–9.
48. Abla N, Naik A, Guy RH, Kalia YN. Effect of charge and molecular weight on transdermal peptide delivery by iontophoresis. Pharm Res. 2005;22:2069–78.
49. Alvarez-Roman R, Naik A, Kalia YN, Guy RH, Fessi H. Skin penetration and distribution of polymeric nanoparticles. J Control Release. 2004;99:53–62.
50. Prausnitz MR, Gimm JA, Guy RH, Langer R, Weaver JC, Cullander C. Imaging regions of transport across human stratum corneum during high-voltage and low-voltage exposures. J Pharm Sci. 1996;85:1363–70.